Materials Science & Engineering C 96 (2019) 776–789

Contents lists available at ScienceDirect

Materials Science & Engineering C

journal homepage: www.elsevier.com/locate/msec

Poly (ε-caprolactone) microspheres for prolonged release of selenium nanoparticles

Nenad Filipović[a], Ljiljana Veselinović[a], Slavica Ražić[b], Sanja Jeremić[c], Metka Filipič[d], Bojana Žegura[d], Sergej Tomić[e], Miodrag Čolić[e,f], Magdalena Stevanović[a,*]

[a] Institute of Technical Sciences of the Serbian Academy of Sciences and Arts, Knez Mihailova 35/IV, 11000 Belgrade, Serbia
[b] Faculty of Pharmacy - Department of Analytical Chemistry, University of Belgrade, 11000 Belgrade, Serbia
[c] Institute of Molecular Genetics and Genetic Engineering, University of Belgrade, 11000 Belgrade, Serbia
[d] Department of Genetic Toxicology and Cancer Biology, National Institute of Biology, Večna pot 111, 1000 Ljubljana, Slovenia
[e] Institute for the Application of Nuclear Energy, University of Belgrade, 11000 Belgrade, Serbia
[f] Medical Faculty of the Military Medical Academy, University of Defence, 11000 Belgrade, Serbia

ARTICLE INFO

Keywords:
PCL
Microspheres
Biodegradation
Prolonged release
Selenium nanoparticles

ABSTRACT

Poly (ε-caprolactone) (PCL) microspheres as a carrier for sustained release of antibacterial agent, selenium nanoparticles (SeNPs), were developed. The obtained PCL/SeNPs microspheres were in the range 1–4 μm with the encapsulation efficiency of about 90%. The degradation process and release behavior of SeNPs from PCL microspheres were investigated in five different degradation media: phosphate buffer solution (PBS), a solution of lipase isolated from the porcine pancreas in PBS, 0.1 M hydrochloric acid (HCl), *Pseudomonas aeruginosa* PAO1 cell-free extract in PBS and implant fluid (exudate) from the subcutaneously implanted sterile polyvinyl sponges which induce a foreign-body inflammatory reaction. The samples were thoroughly characterized by SEM, TEM, FTIR, XRD, PSA, DSC, confocal microscopy, and ICP-OES techniques. Under physiological conditions at neutral pH, a very slow release of SeNPs occurred (3 and 8% in the case of PBS or PBS + lipase, respectively and after 660 days), while in the acidic environment their presence was not detected. On the other hand, the release in the medium with bacterial extract was much more pronounced, even after 24 h (13%). After 7 days, the concentration of SeNPs reached a maximum of around 30%. Also, 37% of SeNPs have been released after 11 days of incubation of PCL/SeNPs in the implant exudate. These results suggest that the release of SeNPs from PCL was triggered by *Pseudomonas aeruginosa* PAO1 bacterium as well as by foreign body inflammatory reaction to implant. Furthermore, PCL/SeNPs microspheres were investigated in terms of their biocompatibility. For this purpose, cytotoxicity, the formation of reactive oxygen species (ROS), and genotoxicity were evaluated on HepG2 cell line. The interaction of PCL/SeNPs with phagocytic cell line (Raw 264.7 macrophages) was monitored as well. It was found that the microspheres in investigated concentration range had no acute cytotoxic effects. Finally, SeNPs, as well as PCL/SeNPs, showed a considerable antibacterial activity against Gram-positive bacteria: *Staphylococcus aureus* (ATCC 25923) and *Staphylococcus epidermidis* (ATCC 1228). These results suggest that PCL/SeNPs-based system could be an attractive platform for a prolonged prevention of infections accompanying implants.

1. Introduction

Degenerative and inflammatory diseases of the bones and joints make half of all chronic diseases in middle age people or older population in developed countries [1]. As a result, millions of medical devices are used every year. However, a significant quantity of these devices becomes colonized by microorganisms leading to implant-related infections, following implant damage and foreign-body reaction [2]. Despite the great progress in the field of biomaterials, this is still a major problem in orthopedics and soft tissue augmentation which causes implants failure. In a study conducted by Mittal et al. [3], > 90% of investigated patients stated that this is the largest drawback of metal implants. Implant accompanied infections are the consequence of bacterial adhesion to implant surfaces triggering the biofilm formation at the implantation site [4]. The formation of biofilms occurs in several phases leading to several major problems. The first problem is that

* Corresponding author.
E-mail addresses: magdalena.stevanovic@itn.sanu.ac.rs, magir@eunet.rs (M. Stevanović).

https://doi.org/10.1016/j.msec.2018.11.073
Received 12 April 2018; Received in revised form 20 November 2018; Accepted 27 November 2018
Available online 29 November 2018
0928-4931/

bacterial populations on implant surfaces may become a reservoir of bacteria that can spread through the whole body. Furthermore, biofilms are highly resistant to antibiotic therapy so it is extremely hard to eliminate these bacteria by conventional antimicrobial therapies. Because the immune system and antimicrobial therapies are often inefficient to eliminate bacteria forming the biofilm, a chronic infection may take place [5]. It is a great challenge to manage orthopedic and soft-tissue augmentation implant infections that can cause implant replacement and also, in severe cases, can lead to amputation and death. About two-thirds of all orthopedic implant infections are initiated by different strains of *staphylococci* [6]. Actually, the most serious problems could be caused by *Staphylococcus aureus* and *Pseudomonas aeruginosa* infections [7]. *S. aureus* bacteria are the major contributing agents of two main infections affecting bone: arthritis and osteomyelitis, which are associated with inflammation and bone destruction [8]. Pseudomonas bacteria usually do not cause severe infections in healthy people [9]. However, infections caused by *P. aeruginosa* are commonly associated with other infections, *i.e.* they often appear in already immunocompromised patients. Pseudomonas is the most frequent pathogen find in patients who have been hospitalized for an extended period of time, and it is a frequent cause of nosocomial infections [10]. Pseudomonas infections often occur, for example, when there is already an existing infection caused by *staphylococci*.

With the aim to prevent postsurgical infection, systemic antibiotic therapy is commonly applied to patients after the implantation [11,12]. However, there are many weaknesses, such as relatively low antibiotic concentration at the target site, as well as potential toxicity [13]. Also, consistent usage of broad-spectrum antibiotics may trigger resistant microorganism infections, which are associated with worse outcomes and higher costs [14,15]. Taking all this into account, coating/impregnation of implants with non-antibiotic antimicrobial substances emerged as a promising approach. However, many currently used non-antibiotic antimicrobial coating materials have been shown to be insufficiently efficient. For example, silver ions, well-known antimicrobial agent, are readily precipitated by chloride ions in human tissues [16]. Also, it should be mentioned that coating devices with silver, gold, and platinum is expensive [17].

On the other hand, SeNPs recently gained attention as a material, which possesses antibacterial, as well as antiviral activities [18–21]. Selenium is an essential trace element in human bodies, required for their normal functioning [22]. Furthermore, recent findings indicate that selenium has critical roles in different physiological processes, including the modulation of immune responses [23] and it is necessary for bone health [24]. The effects of selenium on bone and the underlying mechanisms are well described in the review of Zeng et al. [25]. Selenium deficiency can retard growth, modify bone metabolism and increase the risk of bone disease [25–27]. However, selenium can be also toxic at concentration levels not much higher than the beneficial requirement [28,29]. Conversely, compared to elemental selenium, SeNPs have shown a reduced risk of selenium toxicity, but same bioavailability and efficacy compared with other seleno-compounds [30,31].

Herein, we describe for the first time, the synthesis and characterization of SeNPs encapsulated within PCL microspheres with the aim to establish a system, which will be capable to slow release the SeNPs from PCL matrix on site and when it is needed, *i.e.* when infection or inflammation occurs.

PCL is chosen since it is FDA-approved aliphatic polyester, which belongs to a group of slow-degrading polymers. Some of its numerous applications in the field of biomedicine are summarized in a few review papers [32–34]. Although the majority of researches done with PCL in the past few years are focused on tissue engineering [35], this polymer still has a great potential in drug delivery systems thanks to its excellent biocompatibility [36] or ability to provide sustained release [37]. Also, the slow degradation and prolonged release of active components from PCL could be very beneficial in implant coatings approach. In this case, it is possible to provide antimicrobial protection, prevent disease remission or alter regeneration in a reasonable long period. For such system, degradation rate and release behavior are parameters that must be thoroughly investigated. The degradation rate is highly dependent on several factors including the degree of crystallinity, hydrophilicity, copolymer composition, molecular weight, molecular architecture, size and geometry of the samples, and the conditions in the degradation environment.

In this study, degradation and release behavior of newly synthesized PCL/SeNPs microspheres were investigated in five different media: phosphate buffer solution (PBS), solution of lipase isolated from the porcine pancreas in PBS, 0.1 M hydrochloric acid (HCl), *Pseudomonas aeruginosa* PAO1 cell-free extract in PBS and implant fluid (exudate) from *in vivo* implanted sterile polyvinyl sponges, which induce a foreign-body inflammatory reaction. Samples were characterized by scanning electron microscope (SEM), transmission electron microscope (TEM), Fourier-transform infrared spectroscopy (FTIR), X-ray diffraction (XRD), particle size distribution analysis (PSD), differential scanning calorimetry (DSC) and inductively coupled plasma optical emission spectrometry (ICP-OES). The influence of PCL/SeNPs on cell viability, reactive oxygen species (ROS) generation and formation of DNA strand breaks in HepG2 and phagocytic Raw 264.7 cells was investigated. The antibacterial activity of the samples was determined against Gram-positive bacteria: *Staphylococcus aureus* (ATCC 25923) and *Staphylococcus epidermidis* (ATCC 1228).

2. Experimental section

2.1. Materials

PCL was purchased from Lactel, Absorbable Polymers, USA. Poly (L-glutamic acid) (PGA, MW = 20–40 kDa, 99.9% HPLC purity) was obtained from Guilin Peptide Technology Limited, China. Sodium selenite (Na_2SeO_3, Mw = 172.94 g/mol), bovine serum albumin (MW = 66 kDa, BSA) and lipase (type II 30–90 units/mg protein isolated from porcine pancreas) were obtained from Sigma Aldrich Chemie GmbH. Ascorbic acid (vitamin C) was purchased from VWR Prolabo.

2.2. Synthesis of SeNPs

SeNPs were synthesized by simple chemical reduction, using sodium selenite as a source of selenium ions, ascorbic acid as a reducing agent and BSA as a stabilizer. Droplets of 20 mM solution of sodium selenite (12.5 ml) and 8.6% solution of BSA (w/v, 5 ml) were simultaneously added to 0.125 M solution of ascorbic acid (10 ml). The reaction vessel with ascorbic acid (also where the reduction takes place) was covered with aluminum foil in order to prevent interaction with light. The obtained brick red colloidal solution of SeNPs was homogenized for 30 min on a magnetic stirrer (1000 rpm) and then filtered through the 0.24 μm syringe filter (Millipore). The final solution was stored in a refrigerator. The amount of SeNPs in colloidal solution was determined by ICP-OES. For the purpose of characterization by FTIR, XRD and antibacterial testing, obtained colloidal solution of SeNPs was lyophilized.

2.3. Encapsulation of SeNPs within PCL microspheres

The obtained colloidal solution of SeNPs was further used for encapsulation within PCL microspheres using a solvent/nonsolvent method. Briefly, 300 mg of commercial PCL granules was dissolved with mild heating to 50 °C in 30 ml of acetone. After that, 0.5 ml of a solution containing SeNPs was dropwise added to the organic phase. A high-speed homogenizer was used for 5 min at 21000 rpm to homogenize this mixture. The obtained mixture was poured into a non-solvent system ethanol (75 ml) followed by addition of 0.05% PGA solution (10 ml). This instantly resulted in precipitation of PCL

microspheres loaded with SeNPs. Homogenization was then carried on a magnetic stirrer for 30 min.

The encapsulation efficiency EE% of SeNPs was determined based on the following equation:

$$EE\% = \frac{W_e}{W_t} \cdot 100 \quad (1)$$

where W_e is the amount of incorporated SeNPs within PCL microspheres, determined experimentally by ICP-OES, and W_i is the total quantity of SeNPs added initially during the preparation procedure. In order to thoroughly investigate some properties of obtained PCL/SeNPs, blank PCL microspheres were produced by the same procedure without the addition of SeNPs and high speed homogenization.

2.4. Characterization of the samples

2.4.1. Morphology studies

The morphology of as-synthesized SeNPs and PCL/SeNPs was analyzed by SEM (JEOL JSM-639OLV) and TEM (2100 microscope, Jeol Ltd., Tokyo, Japan). For SEM analysis, the samples were coated with gold using the physical vapor deposition (PVD) process. The covering was performed by a Baltec SCD 005 sputter coater, using 30 mA current from the distance of 50 mm during 180 s. For TEM analysis, samples were prepared by placing drops of suspension-containing particles onto a lacey carbon film supported by a 300-mesh-copper grid.

2.4.2. Fourier-transform infrared spectroscopy (FTIR)

The quality analysis of the samples was performed by FTIR spectroscopy. FTIR spectra of samples were obtained on MIDAC M 2000 Series Research Laboratory FTIR Spectrometer, using the KBr pellet technique. Measurements were performed in a spectral range of 400–4000 cm^{-1} at room temperature.

2.4.3. X-ray diffraction (XRD) measurements

X-ray diffraction spectra were obtained on an X-ray diffractometer, Philips PW 1050 diffractometer with Cu-Kα radiation (Ni filter). The samples were scanned in the 2θ range of 10° to 60°, with a scanning step width of 0.05°, and 2 s per step. Crystallite size determination was carried out using a variant of the Scherrer equation:

$$D = \frac{0.9\lambda}{b\cos\theta} \quad (2)$$

where D is the apparent crystallite size, b is the full-width at half maximum FWHM of the X-ray diffraction line (peak broadening) in radians, λ is the wavelength used 1.5406 Å, and θ is the angle between the incident ray and the scattering planes. The constant of 0.9 is a shape factor and its value depends on crystallite morphology.

2.4.4. Particle size analysis (PSA)

The particle size distribution of SeNPs and PCL/SeNPs samples was determined by the PSA Mastersizer 2000 (Malvern Instruments Ltd., UK). For characterization of SeNPs, the original colloidal solution was used, while particle size distribution of PCL/SeNPs was measured from the powder ultrasonically dispersed in ethanol.

2.4.5. Differential scanning calorimetry (DSC measurements)

DSC studies were carried out on SETARAM apparatus DSC 131 EVO controlled by CALISTO software. In order to evaluate effects of degradation on polymer crystallinity, samples weighing 1,5–2,5 mg were placed in hermetically sealed 30 µl aluminum pans and heated from 30 °C to 100 °C at a rate of 5 °C/min in nitrogen gas flow. The approximate crystallinity was calculated from the melting peak according to the equation:

$$W_c = \frac{\Delta H_f}{\Delta H_f^0} \quad (3)$$

where W_c is the degree of crystallinity, ΔH_f is the heat of fusion of the sample, and ΔH_f^0 is the heat of fusion of 100% crystalline polymer (literature data 139.5 J/g) [38].

2.4.6. Inductively coupled plasma optical emission spectrometry (ICP-OES)

A Thermo Scientific iCap 6500 Duo instrument was used for determination of Se concentration in different samples: colloidal solution of SeNPs, PCL/SeNPs powder and supernatant were taken at predetermined time intervals from different degradation media. Samples in powder form were prepared by microwave acid-assisted digestion. Working solutions of selenium were produced by appropriate dilutions of the corresponding stock solutions with 2.5% nitric acid (HNO_3). Working standards were prepared from the multi-element standard solution, MES-21-1 (AccuStandrad, USA) in following concentrations: 10 ppb, 20 ppb, 50 ppb, 100 ppb, 0,2 ppm, 0,5 ppm, 1 ppm, and 2 ppm. Details of the experimental procedure are given in Supplementary information SI.

2.5. Biocompatibility study

First, the investigations regarding cell viability (MTT assay), the formation of ROS (DCFH-DA assay) and genotoxicity (comet assay) were conducted on the HepG2 cell line. Cell viability after the exposure to PCL/SeNPs was determined with 3-(4,5-dimethylthiazol-2-yl)-2,5 diphenyltetrazolium bromide (MTT) according to Mosmann [39] with minor modifications [40]. The formation of intracellular ROS was measured spectrophotometrically using a fluorescent probe, dichlorodihydro-fluorescein diacetate (DCFH-DA) as described elsewhere [41]. In order to investigate the genotoxicity of PCL/SeNPs, a classical comet assay was performed according to the protocol of Singh et al. with minor modifications [42]. Images of 50 randomly selected nuclei per experimental point were analyzed with image analysis software Comet Assay IV (Perceptive Instruments, UK). The percentages of tail DNA were used to measure the levels of DNA damage. All details regarding biocompatibility testing are provided within SI.

To investigate the interaction between PCL/SeNPs with professional phagocytic cells, murine Raw 264.7 cell line was used, and 2×10^5 cells/well of 24-wells plates were cultivated in complete RPMI 1640 medium with 10% fetal calf serum and 1% antibiotics (gentamycin, streptomycin, penicillin) for 24 h. The cells were then treated with PCL/SeNPs (25, 50 or 100 µg/ml) or PBS (control) for the next 24 h. The viability of cells was analyzed by Tripan blue exclusion assay, by counting at least 500 cells per sample. The % of viable (Tripan blue negative) cells was calculated as the % of control (PBS-treated) cells (100%).

Microscopy analysis of Raw 264.7 cells was carried out on cells cultivated likewise on glass coverslips for 24 h. The slides were washed three times in PBS and then stained with May-Grunwald Giemsa. Alternatively, the samples were stained with the anti-mouse CD45 antibody (Abcam) for 30 min, washed in PBS and then labeled with goat anti-mouse Alexa Fluor 488 IgG (Abcam) for another 30 min. Nuclei were stained afterwards using Syto 59 nuclear stain (Invitrogen), and the samples were analyzed by Zeiss 510 LSM confocal microscope (Zeiss, Jena, Germany). SeNPs were detected as bright scattering particles upon excitation with a 546 nm laser.

2.6. Degradation process and release behavior of SeNPs from PCL microspheres in simulated physiological conditions

The degradation of PCL/SeNPs and the release of SeNps from the PCL polymer matrix were investigated in different degradation media in order to simulate physiological conditions: (i) PBS with pH = 7.4, (ii) PBS solution with lipase isolated from porcine pancreas (3 mg for each sample) and (iii) 0.1 M HCl. All experiments were carried out in parallel. The 15 mg of PCL/SeNp were suspended in 7.5 ml of the abovementioned media and placed in water bath at 37 °C. (sodium azide was

added to the first two media). At exact times, samples were collected, centrifuged (10 min at 7000 rpm) and sediments and supernatants separated by decantation. In order to remove a residue from media, sediments were washed several times with distilled water, filtered through the quantitative filter paper and left to dry at room temperature for two days. All samples were stored in a refrigerator before analysis.

2.7. Study on degradation efficiency of PCL by a Pseudomonas aeruginosa PAO1 cell-free extract

We investigated the ability and the role of *P. aeruginosa* on PCL degradation, using a microcosm approach in order to mimic the bacterial infection conditions. For this purpose, *P. aeruginosa* PAO1 (ATCC 15692) was grown in MSM medium (Mineral Salts Medium) composed of 9.0 g/l $Na_2HPO_4 \times 12H_2O$; 1.5 g/l KH_2PO_4;0.2 g/l $MgSO_4 \times 7H_2O$; 0.002 g/l $CaCl_2$; 1.0 g/l NH_4Cl and 1 ml salt solution [43] supplemented with casamino acids (0.7%, w/v), glucose (0.2%, w/v), or olive oil (1%, v/v) as carbon sources. The bacterial culture was incubated for 48 h at 30 °C with shaking at 180 rpm. After the incubation, *P. aeruginosa* PAO1 bacterial culture was centrifuged at 5000 rpm for 10 min (GS-3 rotor, Sorvall Centrifuge, DuPont Instruments, Delaware, USA) and cell-free extract (CFE) was prepared from the bacterial pellet using BugBuster Protein Extraction Reagent according to the manufacturer's instructions (Novagen, Wisconsin, USA). Total protein concentration in cell-free extract was determined using the coloring reagent CBB G-250 (BioRad Protein Assay, BioRad Laboratories, USA) according to Bradford method [44]. CFE was used in two different experimental setups including semi-solid agar-based medium and aqueous PBS medium.

2.7.1. Degradability potential of P. aeruginosa PAO1 CFE toward PCL

Experiments on agar plates were conducted in order to prove degradability potential of CFE toward PCL. Firstly, a polymer suspension was prepared by dissolving 100 mg of PCL polymer in 2 ml of dichloromethane and water up to 20 ml, followed by sonication (60 Hz, 5 pulses of 1 min) [45]. This suspension was further warmed at 65 °C to evaporate dichloromethane and then mixed with agar (final concentration 1% w/v in 200 mM Tris-HCl buffer pH 8.5) in 1:1 ratio and poured into a glass Petri dish. After solidification at ambient temperature, agar plugs (diameter = 3 mm) were taken out of plates for the addition of cell-free extracts. For the purpose of this experiment, *P. aeruginosa* PAO1 was grown in MSM medium using either glucose or olive oil as carbon sources. Cell-free extracts (50 μl) from both growth media were applied into wells and plates and incubated for 24 h at 30 °C when another aliquot of cell-free extracts (50 μl) was added to wells and plates and further incubated for 3 days at 30 °C.

2.7.2. Influence of P. aeruginosa PAO1 CFE toward PCL/SeNPs in aqueous PBS medium

For experiments in an aqueous medium, 85 mg of PCL/SeNPs powder was suspended in a mixture of 20 mM PBS (8 ml) and *P. aeruginosa* CFE. The experiment was carried out for three weeks at 37 °C. Cell-free extracts (2 ml; 1.8 to 2 mg of total protein/ml) were added in regular periods, three times throughout the duration of the experiment. After 24 h, and at the beginning of the second and third week, before the addition of fresh cell-free extracts, aliquots of 1 ml were taken from the reaction mixture, centrifuged (5 min, 13,000 rpm, Eppendorf Centrifuge 5417C, Hamburg, Germany) and pellets and supernatants stored at −20 °C for further analysis.

2.8. Degradability potential of implant exudate on PCL/SeNPs

To observe whether SeNPs could be released from PCL microspheres during an inflammatory process accompanying implantation, a rat model of sterile inflammation to foreign-body was applied. Namely, Albino Oxford (AO) rats, both sexes, 12 weeks old, were bread at the Institute for Medical Research of the Military Medical Academy (MMA). All animal experiments were approved by the Ethical Committee for Protection of Experimental Animals of MMA. A sterile inflammation to foreign body was induced by subcutaneous implantation of polyvinyl sponges (1 cm × 1.5 cm × 0.25 cm), as described previously [46]. Two sponges per animal were implanted at the dorsal site of the skin, under the general ketamine/xylazine anesthesia. To collect the exudate, animals were sacrificed by the anesthetics overdose, and the sponges were harvested 2 days after implantation. The exudate was squeezed with a syringe and the cells were pelleted by centrifugation (2000 RPM for 10 min). The *in vitro* release of SeNPs from PCL microspheres in cell-free exudate was carried out by incubating PCL/SeNPs (0.5 mg/ml) in the exudate at 37 °C and 5% CO_2 for 11 days, followed by the measurement of released SeNPs with ICP-OES. For the ICP-OES analysis, the exudate was filtered and then the measurements were done directly.

To assess the degradability of PCL/SeNPs *in vivo*, PCL/SeNPs were injected into subcutaneously implanted sponges (totally 4 mg/animal), whereas the control groups received the equivalent amount of sterile PBS. The sponges from control and treated animals were extracted after 3 h, 4 days or 11 days (2 animals per group per time point). The exudate was used for ICP-OES analysis. In addition to standard ICP-OES analysis used to detect released SeNPs, the samples were prepared without filtration, to include SeNPs within PCL in sponges (Total Se) in the exudate. The infiltrating cells isolated from sponges were placed on microscope slides using the cytocentrifuge (Shandon 4, ThermoFisher Scientific), and analyzed by confocal microscopy, as described for Raw 264.7 cells.

2.9. Antibacterial activity

The antibacterial effects of PCL/SeNPs, as well as SeNPs alone, were examined against *S. aureus* (ATCC 25923) and *S. epidermidis* (ATCC 1228). For the determination of minimum inhibitory concentrations (MICs) of the samples a broth microdilution method was used. This is performed according to the Clinical and Laboratory Standards Institute (CLSI 2005) [47]. A serial doubling dilution of the samples was prepared in Müller-Hinton broth over the range of 1000 μg/ml–12.5 μg/ml. In the tests, 0.05% triphenyl tetrazolium chloride (TTC, Aldrich Chemical Company Inc., USA) was also added to the culture medium as a growth indicator. As a positive control of growth, the wells containing only the bacteria in the broth were used. Bacteria growth was determined after 24 h of incubation at 37 °C. All of the MIC determinations were performed in duplicate, and two positive growth controls were included as well.

3. Results and discussion

3.1. Physicochemical characterization of as-prepared samples SeNPs and PCL/SeNPs

The XRD pattern of lyophilized SeNPs revealed that Se was in amorphous form (Fig. 1a). The only peak which can be noticed on the XRD pattern (Fig. 1a) is peak which belongs to BSA which is used in the synthesis of SeNPs as a stabilizer. The concentration of SeNPs in the colloidal solution was estimated by ICP-OES to be 600 ± 61 μg/ml, as calculated from three different batches. Morphology and size of nano- and microparticles along with surface chemistry are one of the most influential parameters that determine their fate within biological systems [48–50]. One of the major requirements for the controlled and well-balanced release of the drugs in the body is its ideal spherical shape of the particles and narrow distribution of their sizes [17]. A report from particle size distribution measurement of SeNPs indicates that 50% of particles have a radius below 57 nm, while 90% of them are smaller than 97 nm (Fig. 1b). The Fig. 1c, TEM image obtained from Se colloidal solution, shows that SeNPs are quite uniform and spherical with a diameter below 100 nm. The stability of the colloidal solution,

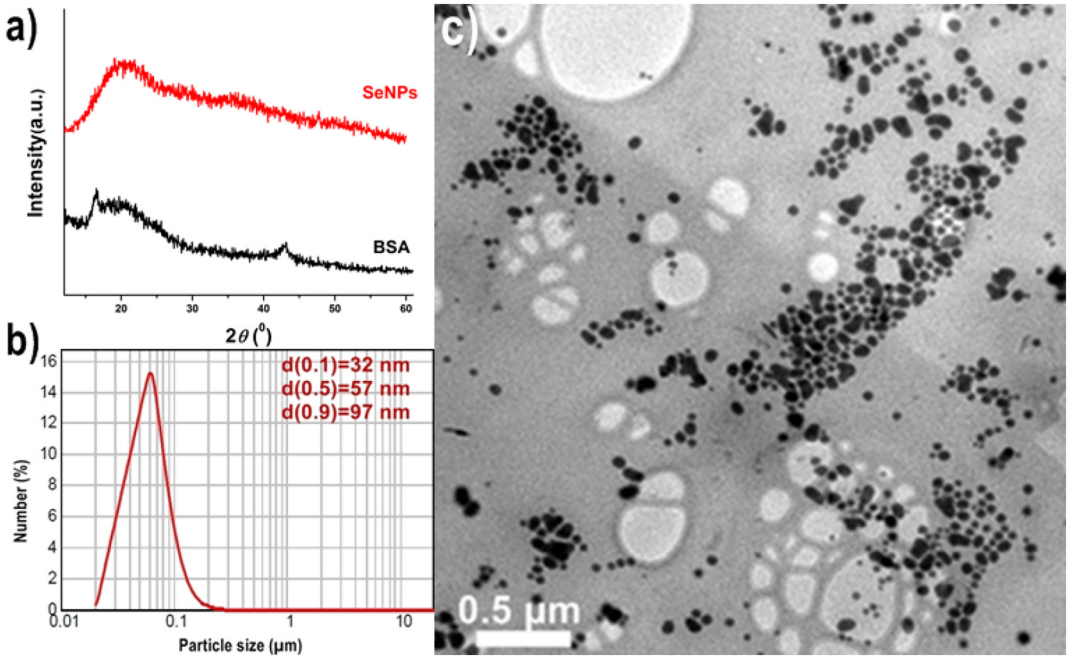

Fig. 1. a) XRD spectra of as-prepared SeNPs and commercial BSA which is used as a stabilizer for SeNPs; b) Size distribution of SeNPs; c) Representative TEM image of SeNPs.

stored in a refrigerator, is estimated to be at least four months, based on the appearance of turbidity.

When it comes to PCL/SeNPs, SEM image confirmed the presence of microspheres within the size range of 1–4 μm (Fig. 2a). SEM image of blank PCL microspheres is given in SI as Fig. 1. PSA is in good agreement with SEM micrograph. Fifty percent of microspheres have a diameter smaller than 1.7 μm, while 90% are below 3.2 μm (Fig. 2b). PCL microspheres loaded with SeNPs were also analyzed by TEM in order to examine the internal structure of such particles, *i.e.* to visualize SeNPs within a polymer matrix. As shown in Fig. 2c and d, SeNPs were randomly distributed within a PCL polymer matrix. Based on Eq. (1) given above, the EE% was calculated to be 90.2% while the loading amount of Se in the PCL/SeNPs system was determined to be 0.0946%. Controlled release systems such as PCL/SeNPs can be an effective means for local

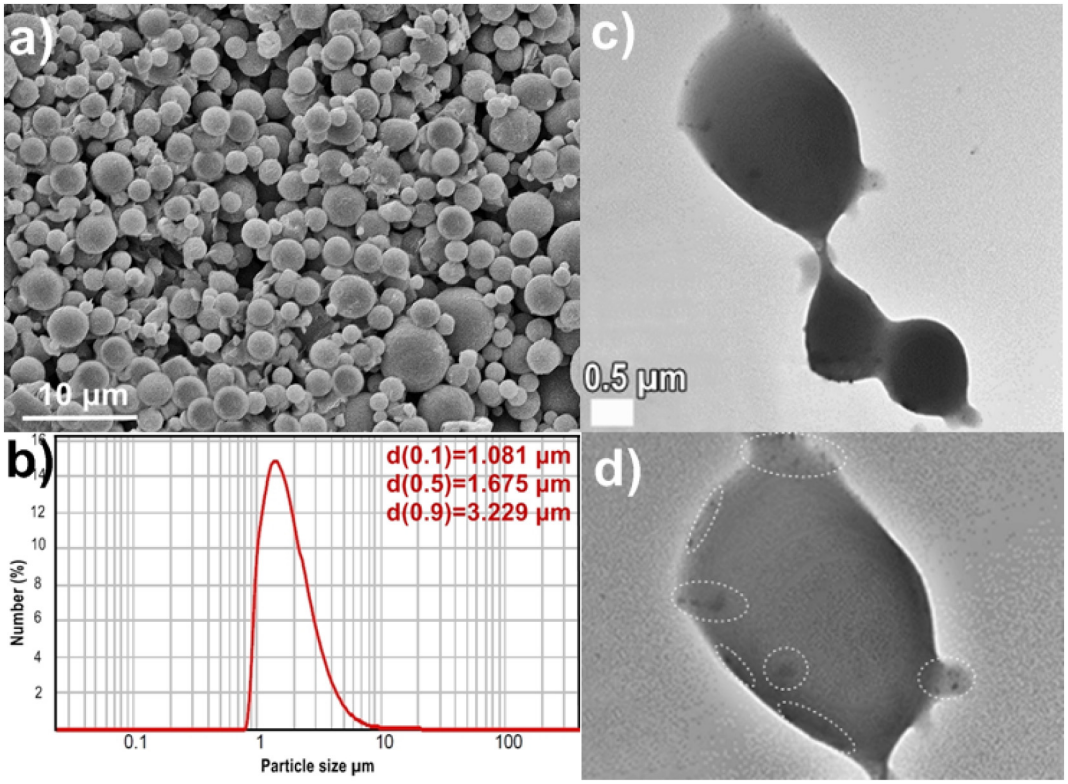

Fig. 2. Morphology of PCL/SeNPs microspheres by SEM, TEM and PSA results. a) Representative SEM image of PCL/SeNPs. b) Size distribution of PCL/SeNPs. c) Representative TEM image of PCL/SeNPs. d) An enlarged individual particle from image "c" with marked SeNPs (dark spots) within the PCL polymer matrix.

drug delivery. In local drug delivery, the main goal is to supply therapeutic levels of active substances at a physical site in the body for a prolonged period. A second goal is to reduce systemic toxicities [51]. Although selenium is needed for the normal functioning of the body, the problem is that it displays a narrow spectrum between favorable and toxic effects [28,29]. According to the U.S. Food and Drug Administration (FDA) recommended dietary allowances (RDAs) of selenium is 55 μg for adults [52], while the National institutes for health (NIH) consider 400 μg of selenium as the tolerable upper intake level (ULs) *i.e.* maximum daily intake unlikely to cause adverse health effects [53]. In the case of our system, this amount will be accomplished with roughly 420 mg of PCL/SeNPs powder. Also, the additional aspect of SeNPs loading amount, which we have considered is the fact that, in this case, there is no significant amount of Se adsorbed on the surface of PCL microspheres and hence no accompanying burst release. This is very important since eliminates the possibility of a potential initial local toxic effect of SeNPs so the system can be considered as safe for prolonged release. TEM images show that SeNPs nanoparticles are heterogeneously dispersed within the PCL and near the edge of these microspheres, but it is not clear whether they are more concentrated in that part. A possible reason why only a few SeNPs are notable on the periphery of the PCL particles is because the thickness of the PCL particles is lowest there, while the central part of the particles is thicker so the difference in material density cannot be detected. Solvent/non-solvent method is a very convenient synthesis technique, frequently used in drug delivery systems. The main requirements are a good choice of polymer solvent, which is also miscible with polymer non-solvent (usually water). The ratio of solvent to non-solvent and choice of stabilizing agents are dominant factors that determine the morphology and size of the particles. In our previous work, PGA has proved to be a good stabilizing agent for obtaining PCL submicron particles [54]. It is characterized by good biocompatibility and adhesive properties which allow its application in the food and pharmaceutical industry, even as a component of surgical glues [55,56].

The further analysis of the PCL/SeNPs was performed by FTIR, XRD, and DSC techniques. FTIR spectroscopy is a very useful technique to investigate the interactions of functional groups based on the shift of vibrational bands. Based on the analysis of the spectra of PCL, PCL/SeNPs and SeNPs (Fig. 3a), there is no indication of chemical interaction between PCL and SeNPs. This leads to the conclusion that SeNPs are physically entrapped within the polymer matrix. All bands that appeared on spectra obtained for blank and loaded PCL particles are characteristic and well recognized for this polymer such as C═O at 1730 cm^{-1}, CH symmetrical and asymmetrical vibrations at 2868 and 2947 cm^{-1}, respectively, C—O at 1173 cm^{-1} *etc.* [57]. On the spectrum obtained from lyophilized SeNPs, two dominant absorptions of IR radiation take place at 3425 cm^{-1} and 1635 cm^{-1}. The first one corresponds to stretching vibrations of H atoms covalently bounded to oxygen or nitrogen atoms and probably hydrogen bonded between other atoms, as well. The second broad peak can be characterized as amide I band. Both bands are characteristic for BSA [58].

The XRD patterns of blank and loaded PCL microspheres are given in Fig. 3b. On both diagrams, two dominant peaks come from diffraction from (110) and (200) crystalline planes [59]. It is noticed a slight shift in 2θ values from 21.55° and 23.85° for the blank polymer to 21.65° and 23.95° for polymer loaded with SeNPs, respectively. Besides these diffraction peaks, a peak of small intensity at 26.1° 2θ, that originates from PGA was also noticed (SI Fig. 2). One can also observe that the baseline for the sample containing SeNPs, is slightly lifted (1.28×) in the 2θ interval 17–25°. A possible explanation for this phenomenon could be the presence of amorphous species in this sample *i.e.* SeNPs. The crystalline regions in polymers are usually composed of crystallites with nano-scale thickness. According to the Scherrer equation, the crystallite size decreased from 208 Å for blank PCL to 180 Å for PCL/SeNPs. Calculations were made for both peaks with excellent matching for PCL/SeNPs and slight inconsistency for blank PCL (for the second peak coming from (200) plane, size of crystallites was estimated to be 216 Å).

The crystallinity of polymers is a very important property, which often correlates with their mechanical properties. For biodegradable polymers, such is PCL, the crystallinity was also shown to have a significant influence on the degradation mechanism and rate [60,61]. DSC is a useful technique for the determination of polymer crystallinity based on enthalpy of polymer melting. Also, it could be used for assessment of interactions between a constituent of an investigated system based on the change of melting enthalpies and on the shift of the melting temperature. Melting of polymers is quite different compared to the melting of pure crystalline materials and always happens in a broader temperature interval. The broadness of melting endotherms could be correlated with a distribution of lamella thickness and imperfections of crystalline domains. Melting enthalpies of blank and loaded particles are 84.5 J/g and 76.8 J/g (Fig. 3c) which corresponds to the degree of crystallinity of 60% and 55%, respectively. The melting temperature is shifted from 64.9 °C for the blank sample to 63.6 °C for a sample containing SeNPs (Fig. 3c). The decrease of crystallinity along with the decrease in melting temperature suggests that the addition of SeNPs colloidal solution during the synthesis procedure promoted the formation of the amorphous region and caused the slight decrease in the thickness of lamella. The confirmation of these results can be found in those obtained for crystallite size from XRD measurements.

3.2. Biocompatibility study

The biocompatibility and safety of PCL/SeNPs were tested with the combination of several methods, namely MTT and comet assay, respectively, while the influence on the formation of ROS was assessed with DCFH-DA method (Fig. 4). The PCL is one of the synthetic polymers recognized as biocompatible and bioresorbable by leading world organizations such as FDA. On the other hand, as it was already mentioned above, besides its beneficial effects, selenium is considered as a very toxic material so its biomedical application is often limited and requires great precautions. In our previous work, we reported that blank PCL particles have no toxic effects toward HepG2 cells [57]. For PCL particles loaded with selenium, similar results were obtained. The only difference noticed was a slight drop of viability after 24-hour exposure to PCL/SeNPs; however, the decrease of cell viability compared to solvent control was approximately 20%, which is still considered not to be cytotoxic (ISO 10993-5:2009). In addition, no concentration dependent reduction of cell viability was obtained. The reason for this effect could be the presence of SeNPs, which might affect the cell growth and division rather than inducing the direct cytotoxic effect. On the other hand, neither ROS formation (during 5 h exposure) nor DNA strand breaks induction were detected after 24 h exposure of HepG2 cells to PCL/SeNPs at the applied conditions. Furthermore there is no clear concentration dependency in causing cytotoxic effects, increasing level of ROS or DNA damaging that will indicate a burst release or desorption of SeNPs from the surface of PCL microspheres (Fig. 4).

The first cells to arrive at the site of implantation and infection are professional phagocytes, such as granulocytes and macrophages [2]. Thereby, the intracellular PCL/SeNPs could behave differently and induce cytotoxicity upon their internalization. Therefore, we also tested whether PCL/SeNPs can induce cell death of Raw 264.7 murine macrophages after 24 h *in vitro*. Expectedly, Raw 264.7 cells were able to internalize smaller PCL/SeNPs, whereas the larger ones were surrounded by Raw 264.7 cells and were located extracellularly (Fig. 5a). Due to their surface plasmon resonance at 520 nm [62], SeNPs could be detected by confocal microscopy as strongly scattering nanoparticles upon 546 nm laser excitation. The analysis confirmed that smaller PCL/SeNPs were indeed localized within Raw 264.7 cells, as well as outside the cells. SeNPs were largely confined within the PCL microspheres irrespective of their intracellular localization.

Moreover, the viability of Raw 264.7 cell was not decreased for >

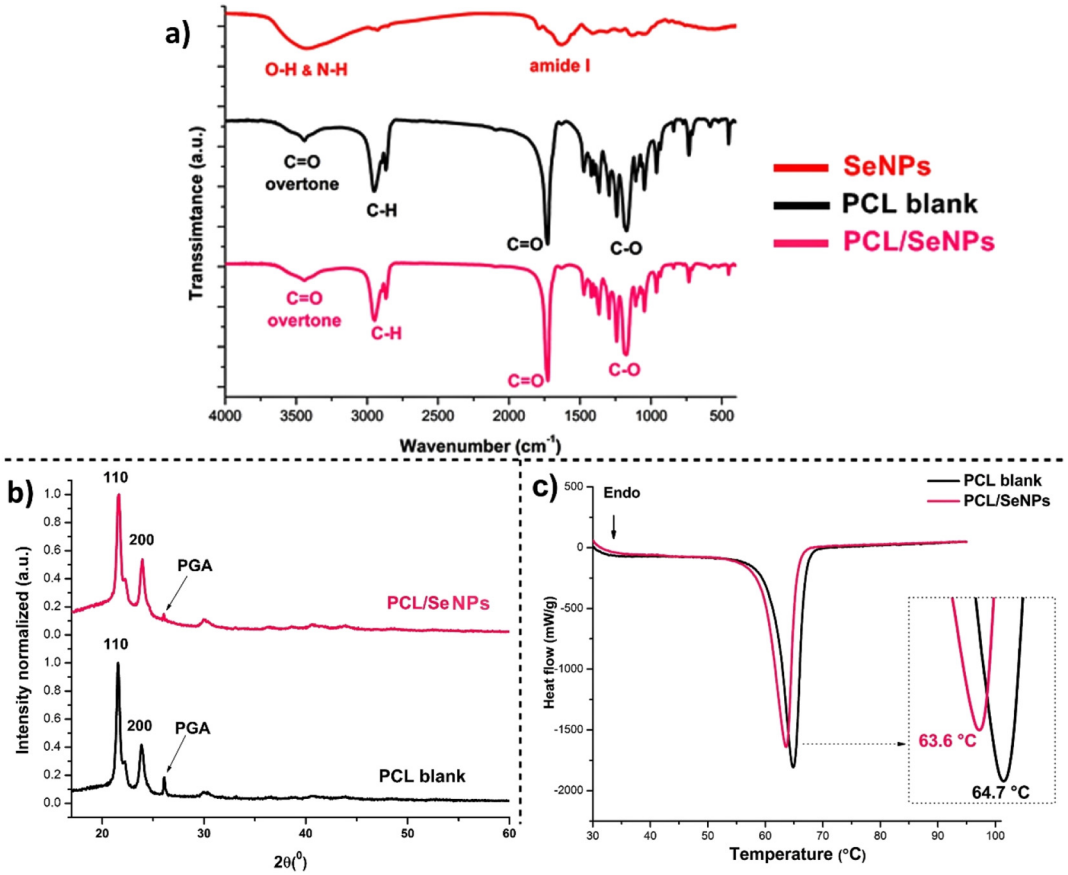

Fig. 3. Analysis of PCL/SeNPs by FTIR, XRD, and DSC. a) FTIR spectra of as-prepared SeNPs, PCL blank particles, and PCL/SeNPs. b) XRD spectra of blank PCL particles and PCL/SeNPs. c) DSC diagrams of PCL blank particles and PCL/SeNPs.

20% after 24 h cultures at the highest concentration used 100 μg/ml (0.01 v/v%) in these experiments, suggesting a lack of significant cytotoxicity for phagocytic Raw 264.7 cells (Fig. 5b). These results suggested that there is no significant release of SeNPs from PCL within 24 h, even upon the internalization. However, to confirm this hypothesis, more sensitive techniques should be applied to study the intracellular release of SeNPs from PCL.

3.3. Degradation studies

3.3.1. Calorimetric studies

Before starting our discussion, it should be emphasized that all samples were taken from the same batch so all of them had same starting morphology, microstructure, percent of crystallinity, and the same amount of SeNPs (assuming a homogeneous distribution of SeNPs). Therefore, we can conclude that the sample degradation rate and release of SeNPs was influenced only by the media nature. DSC diagrams of the samples suspended in phosphate buffer solution (PBS), PBS with lipase isolated from porcine pancreas and 0.1 M HCl are given in Fig. 6.

Although DSC is not very precise and is often mistakenly considered as a technique for routine measurements of phase transitions, it provides useful data for interpretation of polymer structure and interactions based on the shape of the melting/crystallization curves. Generally, the more imperfect polymer crystals are and the wider distribution of lamella thickness is, the more irregular shape of the melting curve will be recorded (broadness of the peak, asymmetrical profile, shifting of melting point, *etc.*). If we compare diagrams obtained for each medium, we could observe the difference in shapes for samples taken after one week and at the end of experiments. Melting endotherms measured after one week were quite symmetrical, while those obtained at the end of experiments were irregularly shaped in a lower temperature range. This irregularity slowly evolves with degradation time in pH-neutral media (Fig. 6a and b) while in the acidic medium (Fig. 6c), it appears only at the end of the experiment and is less pronounced. The appearance of shoulders in lower temperature parts of the peaks could be related to the bimodal distribution of lamella thickness. The melting peak temperatures and corresponding heat of fusions are given in SI Table 1. It is evident that melting temperature and heat of fusion increase with degradation time since degradation first takes place in amorphous regions. By comparing the values of crystallinity slightly higher values were noticed in samples taken from PBS + lipase between 5th and 15th week. The overall increase in crystallinity is almost the same for all media, about 15% in total.

3.3.2. X-ray diffraction studies

Compared to Fig. 3b, the first notable change in all XRD patterns (Fig. 7 a-c) is a disappearance of PGA diffraction peak, which is probably due to PGA desorption from PCL surface during the degradation process. The stabilization effects of PGA on the PCL surface were previously determined in a similar system [54]. However, the interaction between these two polymers seems to be insufficient to overcome PGA desorption due to hydrophilic interactions with water. The second conclusion based on observation of all XRD patterns is that there is no formation of new crystalline phases or a significant change in crystallinity during the degradation period. As shown by Pinto et al. [63], amorphous selenium spontaneously crystallizes during storage at room temperature. However, this behavior is not observed in our system presumably because a stabilization effect of BSA is preserved in hydrophobic PCL environment. In order to closer investigate changes in the crystalline structure of PCL, the Scherrer equation was employed and results for crystallite size are presented in Fig. 7. Calculations were

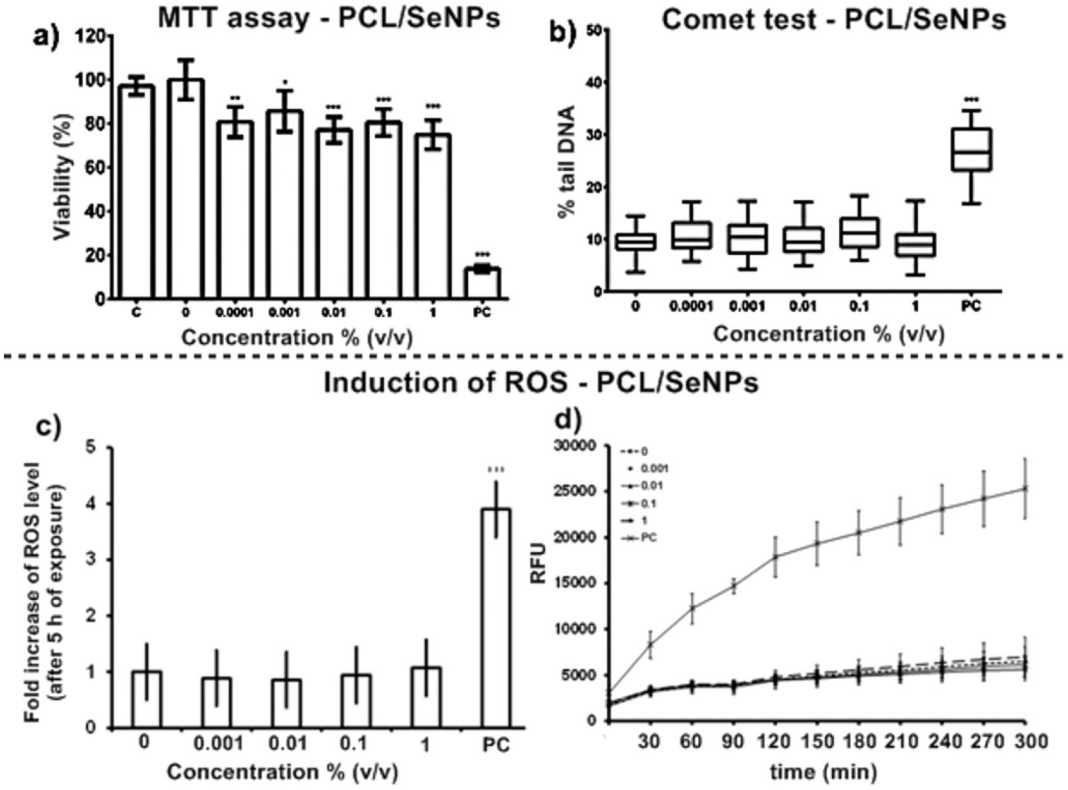

Fig. 4. Biocompatibility studies of PCL/SeNPs. a) MTT assay for different concentration of PCL/SeNPs control (cells exposed only in growth media) and positive control (PC - etoposide 125 μg/ml); b) Comet assay - genotoxicity of PCL/SeNPs SeNPs investigated at the same concentrations and time point as in the MTT assay. As a positive control, benzo[*a*]pyrene (BaP) was used at a concentration of 30 μM. Data for the control are not included since there was no difference between them and those obtained for the solvent control; c) The induction of ROS formation after 5 h exposure to a different concentration of PCL/SeNPs. The data for the control were excluded since there was no difference between them and those obtained for the solvent control; d) Relative fluorescence units RFU measured at every 30 min over 5 h for PCL/SeNPs concentrations from 0 to 1.

made for both peaks present in XRD patterns ((110) and (200)). The use of this equation is still a primary technique for gaining insight into a lamellar thickness in polymer crystallites. On the other side, polymer crystallites often display a relatively large number of defects. This can lead to broadening of diffraction peak and further diminish the accuracy of obtained results. As already mentioned, if we consider that all starting parameters for samples are equal, we can determine relative change of crystallite size with degradation time. Crystallite sizes obtained from (200) plane reflections are generally lower by 20–40 Å than those calculated from 110 plane reflections, however, they both change with degradation time in a similar manner. The exception is noticed only for PBS medium where changes in crystallite size during the first 5 weeks are opposite. Major changes in crystallite size occurred between 2nd-7th weeks for all media, and afterwards monotonously increased to reach their final values. The overall change in crystallite size calculated from the first peak was 209–230 Å, 215–223 Å and 213–228 Å for samples taken from PBS, PBS with lipase and HCl respectively. For the second peak, the crystallite size of samples taken after one week is much closer to the values obtained initial samples. The overall change in the crystallite size goes from 187 Å to 202 Å in the case of PBS as degradation medium, from 170 Å to180 Å in the case of PBS with lipase, and for the acidic medium, one can even notice a small drop in crystallite size from 189 Å to184 Å. Although there is a small inconsistency between the changes of crystallite size calculated from different peaks, we can reach the following conclusions. Broadening of diffraction peaks happened between 14 and 50 days. This broadening is most pronounced for the sample suspended in an acidic medium for 5 weeks. As degradation continued, peaks narrowed, and at the end of the experiment size of crystallites increased on average 5–10%. Castilla-Cortázar et al. reported similar results for PCL networks during degradation in medium with Pseudomonas lipase [59]. Conversely, in the same study, it is observed a constant decrease of crystallite size in PBS.

3.3.3. Degradability potential of P. aeruginosa PAO1 CFE toward PCL and PCL/SeNPs

In order to examine the influence of *P. aeruginosa* PAO1 CFE on the degradation of PCL, experiments on agar plates were conducted. Zone of clearance around wells in the agar plate indicates the enzymatic degradability of the PCL polymer (Fig. 8a.). In case of the CFE of culture grown on olive oil used as carbon source, a greater clearance zone was obtained (radius 10.5 mm) compared to the case when glucose was carbon source because higher esterase titer was induced under these growth conditions.

The change of melting endotherms of PCL/SeNPs with degradation time is most clearly notable for the medium which contains *P. aeruginosa* PAO1 CFE (Fig. 8). The evolution of shoulder in the lower temperature segment of the peak was visible even after 7 days of degradation, while in the media which simulate physiological conditions this phenomenon was prominent only for the samples taken after 108 and 660 days from degradation media. The overall increase in melting peak temperatures was 2.6 °C, which is comparable with experimental results for previous media, but with about 2 °C lower temperatures (SI Table 2). When it comes to crystallinity degree, the value obtained for the sample taken after one day was 53% and afterward increased to 68% or 15% in total. These results are in a good agreement with those obtained for the first three media. Based on the DSC measurements, degradation effects such as an increase in crystallinity and bimodal distribution of lamellar thickness were achieved in the medium which contained *P. aeruginosa* PAO1 CFE after 3 weeks, while same effects

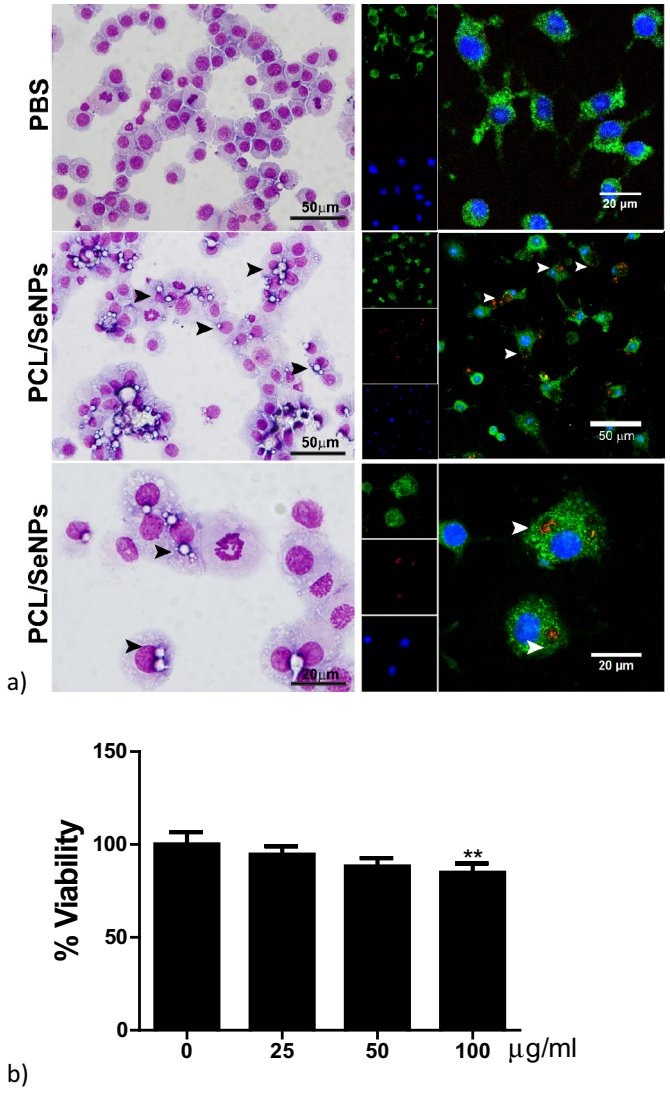

Fig. 5. Interaction of PCL/SeNPs with Raw 264.7 cells. a) Raw 264.7 cells were cultivated with PCL/SeNPs (50 µg/ml) on glass coverslips or without them (control), followed by staining with MGG (left column), or anti-CD45/IgG Alexa 488 (green) and Syto59 nuclear stain (blue) (right column). SeNPs were detected as brightly scattering particles after 546 nm laser excitation. Arrows point to extracellular or intracellular PCL/SeNPs. b) Viability of Raw 264.7 cells after PCL/SeNPs exposure was determined after 24 h cultures with PCL/SeNPs (25, 50 or 100 µg/ml). After that, the cells were harvested and the viability was determined by Tripan blue exclusion test. The results are shown as mean ± SD ($n = 3$ measurements) of viability relative to control non-treated cells (100%), from a representative experiment out of two with similar results. $^{**}p < 0.01$ compared to control (0 µg/ml). (For interpretation of the references to colour in this figure legend, the reader is referred to the web version of this article.)

were noticed in the first three media only after 660 days of degradation.

3.4. In vitro release behavior of SeNPs from PCL microspheres

The release of versatile drugs from PCL microspheres have been thoroughly investigated in the past. Details of these studies are summarized in a few excellent review papers [32–34]. Diffusion of drugs from the microsphere matrix is recognized as a dominant mechanism of drug release from PCL [34]. For this reason, drug distribution within polymer microspheres has a significant influence on the drug diffusion rate. For instance, drug molecules distributed closer to the microsphere surface diffuse out faster from the polymer matrix. Encapsulation of a hydrophilic drug within a hydrophobic polymer, such is PCL, usually results in drug molecules distributed closer to the polymer surface [64].

Another important aspect in drug release is degradation medium. Accelerated degradation could be achieved using an acidic/basic medium, or medium with adequate enzymes, which would enhance the hydrolysis of polyesters and better mimic physiological conditions than temperature degradation, for instance. The surrounding conditions, such as neutral or low pH, had different effects on SeNPs release during the degradation period in such manner that acidic environment inhibited SeNPs release (Fig. 9.). To the best of our knowledge, such behavior has not been reported so far in the literature. A possible explanation for this phenomenon is related to BSA conformation under the acidic conditions. Generally, a low pH causes unfolding of the BSA molecule. These conformational changes can further prevent passage of BSA with SeNPs through diffusion channels and release from the polymer matrix. Suppression of BSA release in the acidic environment was already shown with PLGA microparticles [65]. As expected, the presence of porcine pancreas lipase accelerated SeNPs release, but not in significant amount, from 2 to 8%. On the other hand, a two-fold increase in SeNPs release was noticed in *Pseudomonas* extract after only 24 h and proceeded to its maximum value of around 30% after 7 days. During the following two weeks, the concentration of SeNPs in supernatant did not increase further. On the opposite, a small drop in SeNPs concentration was noticed, probably due to SeNPs adsorption on the polymer surface. Lipase isolated from *Pseudomonas* are well known for their ability to significantly accelerate the degradation of PCL [66,67]. For the first time in this work, a CFE, instead of a single isolated enzyme was used to better mimic the bacterial environment. Enzymatic biodegradation occurs mainly on the surface because it is difficult for these high molecular weight molecules to diffuse into a hydrophobic polymer. A reasonable explanation for the existence of the release profile plateau in Fig. 9b is that all of the released SeNPs originate from regions that are amorphous and close to microsphere surface, which allows them to diffuse out faster from the polymer matrix. Conversely, the remaining amount of SeNPs (around 70%) is deeply incorporated and located closer to crystalline phases. In order to release the remaining amount of SeNPs degradation process had to reach its final stage, *i.e.* breaking the polymer chains to soluble oligomers. Another possible explanation could be that some amount of SeNPs coated with BSA formed agglomerates which are not capable to diffuse out from the polymer matrix.

Bearing in mind results obtained from DSC and XRD measurements some correlations can be made regarding SeNPs release in different degradation media. Degradation processes such as the formation of diffusion channels probably produce some crystallite defects which further cause alteration of FWHM on XRD patterns. On the other hand, DSC technique is not sensitive enough to detect those initial degradation changes but it is still useful for detecting the change in crystallite size distribution as an evidence of advanced degradation when diffusion channels are well formed. In addition, the higher values of crystallinity noticed between 5th and 15th weeks in the medium PBS + lipase, as a consequence of higher degradation rate of amorphous regions, resulted in an increase in SeNPs release.

3.5. The release of SeNPs in implant fluid (exudate)

The release of SeNP from PCL was measured in implant fluid (exudate) extracted from the subcutaneously implanted polyvinyl sponges which induce a sterile inflammation as a part of foreign body reaction, as we described previously [46]. After 11 days of incubation of PCL/SeNPs at 0.5 mg / ml of exudate, ICP-OES analysis showed that 37% of SeNPs have been released. This level is comparable to the values obtained in the medium with *P. aeruginosa* bacterial extract where the concentration of SeNPs reached a maximum value of around 30% after seven days.

To test the release of SeNPs *in vivo*, 4 mg of PCL/SeNPs were injected in the sponges implanted subcutaneously into rats, followed by

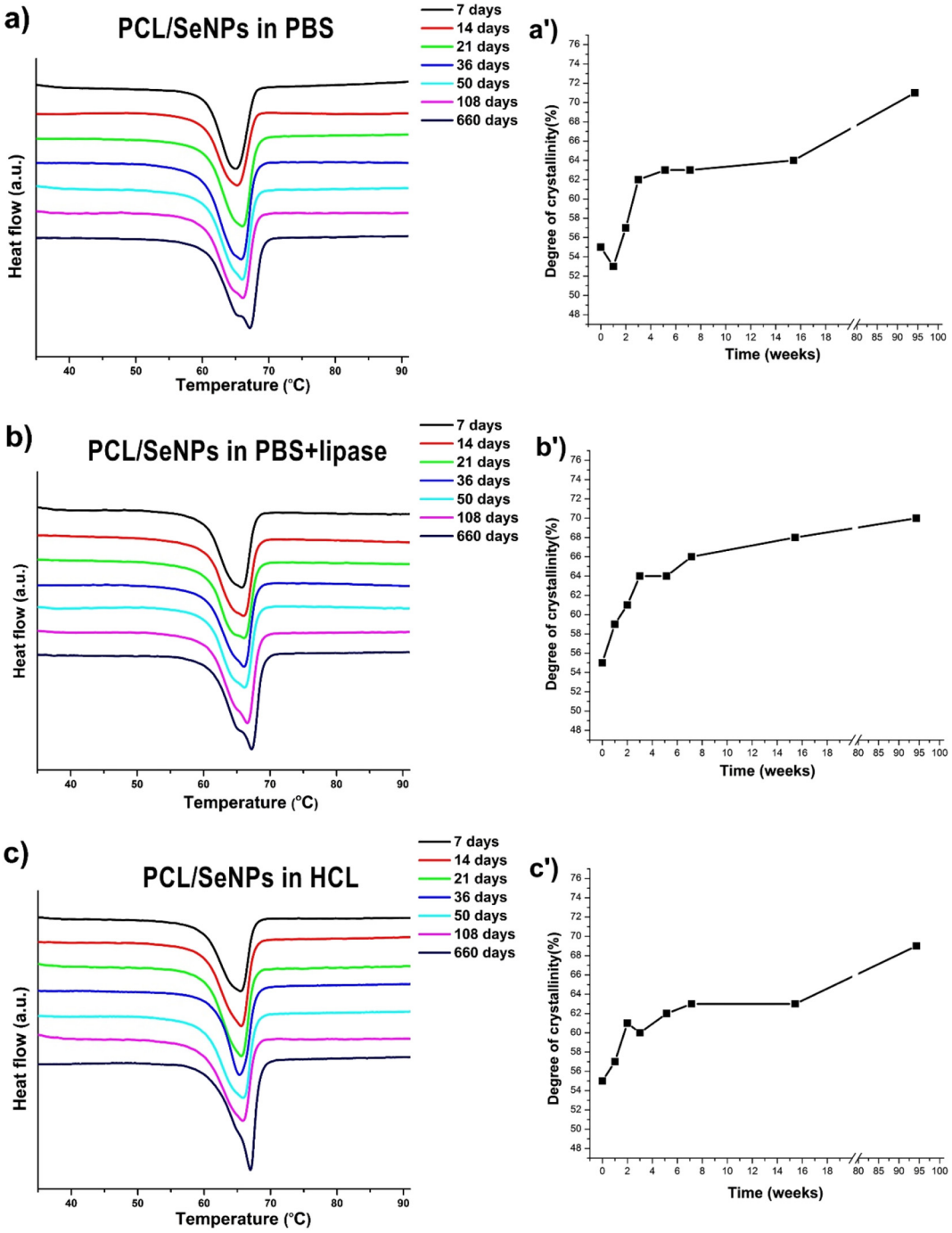

Fig. 6. DSC melting curves of PCL/SeNPs taken at predetermined time intervals from different degradation media: a) PBS, b) PBS with lipase and c) 0.1 M HCl. The time intervals were: 7, 14, 21, 36, 50, 108 and 660 days, respectively, from the highest to the lowest curve on each graphic. The change of crystallinity with degradation period for corresponding media are given as a′), b′) and c′).

the extraction of sponges after 3 h, 4 days or 11 days from the animals. At 3 h time point, the total concentration of Se detected by ICP-OES analysis was shown to be 9%, and the presence of brightly scattering particles sized around 1–4 μm (PCL/SeNPs) was also detected by confocal microscopy within the infiltrating $CD45^+$ cells or extracellularly (SI Fig. 3).

The levels of total Se (released or contained within PCL) were undetectable in the extracted sponges after 4 and 11 days post injection. These results suggest that the PCL/SeNPs were not contained within the sponges, and where probably distributed by lymphatics throughout the body. Therefore, to better study the release of SeNPs from PCL *in vivo*, a kind of scaffold biomaterial would be a better model than the porous polyvinyl sponges, so additional investigations are required to resolve the dynamics of SeNPs release form PCL microspheres *in vivo*.

3.6. Antibacterial activity

Although SeNPs are not recognized as a strong antibacterial agent, an increased scientific interest on this topic was noticed in the last several years. One of the main reasons for this growing interest are findings that elemental nano-Se expresses lower toxicity compared to other Se compounds and that this microelement is normally present in

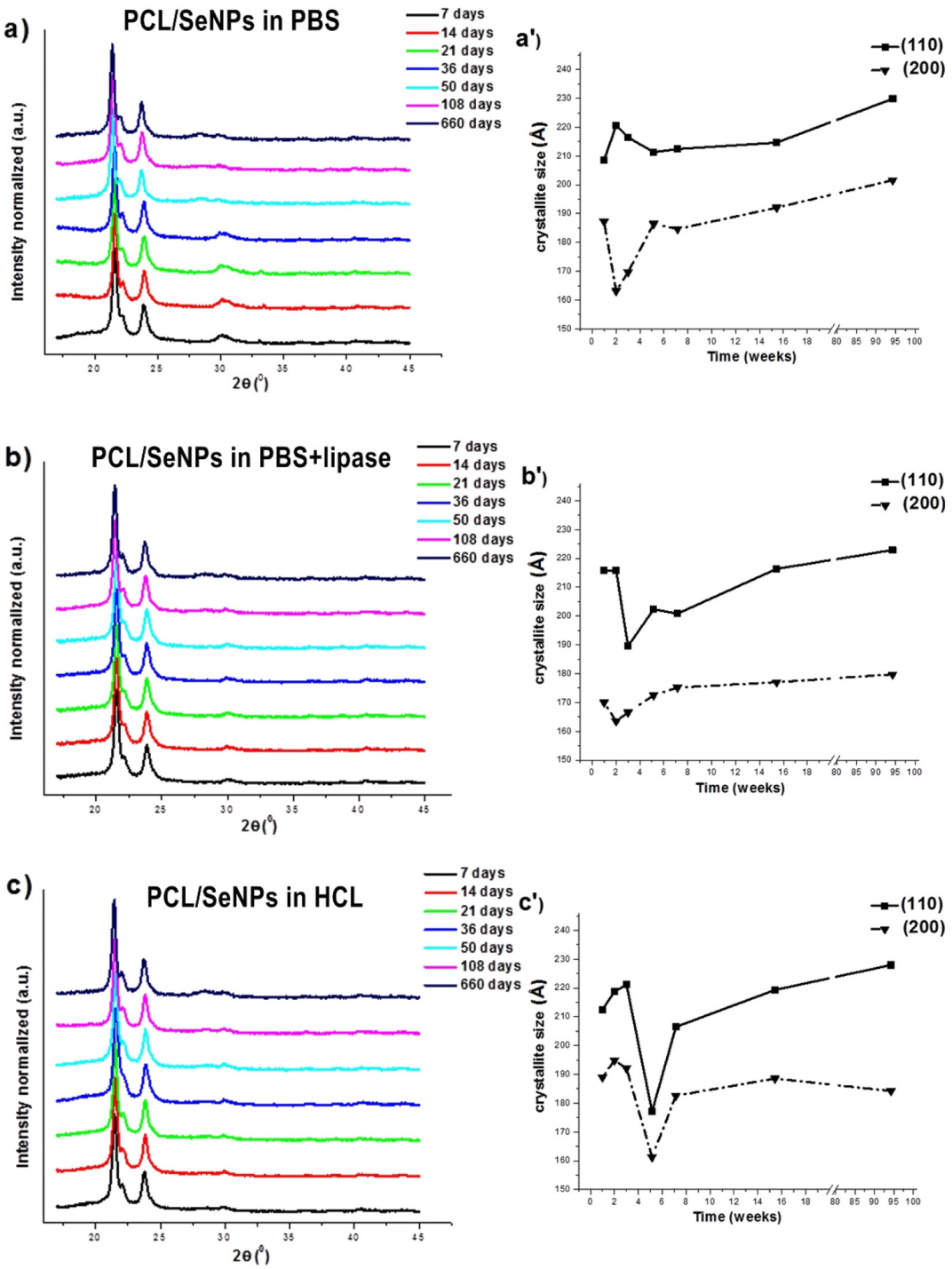

Fig. 7. XRD patterns of PCL/SeNPs for samples taken at predetermined time intervals from different degradation media: (a) PBS, (b) PBS + lipase, and (c) 0.1 M HCl. The time intervals were:7, 14, 21, 36, 50, 108 and 660 days respectively from the lowest to the highest diffractogram on each graphic. The change of crystallite size with time for corresponding media is given as a′, b′ and c′. The calculation was done for both crystalline planes (110) and (200).

our bodies and very important for our health compared to other popular antimicrobial agents, such as Ag. Results of antibacterial activity of SeNPs as well as for PCL/SeNPs are presented in Fig. 10. Minimum inhibitory concentration (MIC) is defined as the lowest concentration of a compound at which a microorganism does not demonstrate any visible growth. One can see that the SeNPs antibacterial effect against *S. aureus* was twice stronger compared to that against *S. epidermidis*. These results are similar to those obtained by other authors [21,68] and show that SeNPs have a good potential for the prevention of infections caused by investigated bacterial strains. Results of this study (Fig. 10) also provided evidence of a considerable antibacterial activity against both bacterial strains, in the presence of PCL/SeNPs as well. This probably can be explained also due to the fact that the PGA used for the stabilization of the PCL/SeNPs also has antimicrobial properties since it is a polyelectrolyte. The potent bactericidal activity of polyelectrolytes could be explained by their strong interaction with the charged cell membrane of bacteria [69]. Furthermore, in our study, the antibacterial activity of SeNPs is achieved with 125 and 250 μg (Fig. 10) which further mean that 133 mg and 265 mg of PCL/SeNPs powder could be sufficient to prevent bacterial growth.

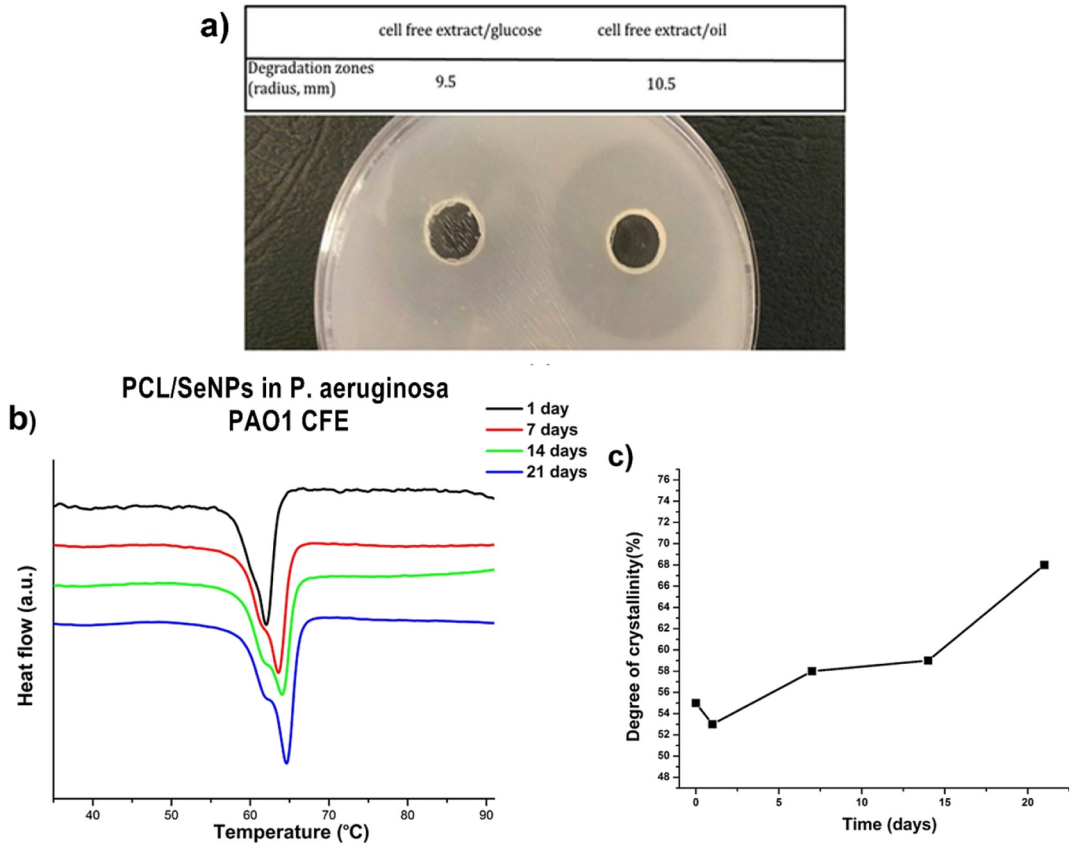

Fig. 8. a) Zone of clearance around wells in the agar plate as an indication of the enzymatic degradability of the PCL polymer. b) DSC heating curves of PCL/SeNPs as a function of time of the degradation in PBS with *P. aeruginosa* CFE c) Crystallinity grade analysis by DSC of the samples as a function of time of the degradation in PBS with *P. aeruginosa* PAO1 CFE.

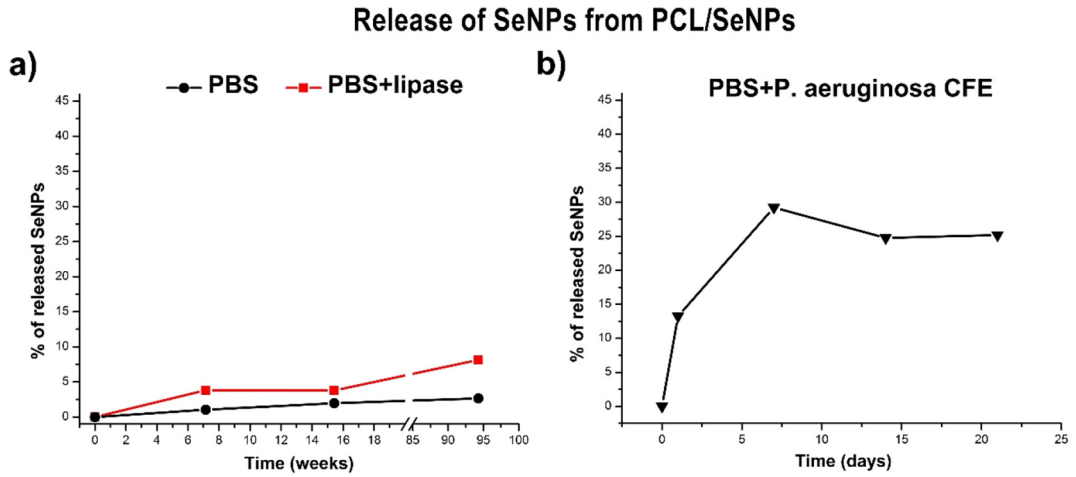

Fig. 9. The release of SeNPs from different degradation media. a) Parallel view of release from PBS and PBS with lipase; b) Release from a medium which contains *P. aeruginosa* PAO1 CFE. For better comparison, the same scale was used for "y" axes in both graphics.

4. Conclusion

From the application aspect, degradation of biodegradable polymers and release of active components are one of the most important properties of polymer-based drug delivery systems. Unique PCL microparticles with incorporated selenium nanoparticles (PCL/SeNPs) were developed aiming to prevent infections on implants. Regarding the SeNPs release from PCL microspheres, encapsulation process and choice of stabilizing agent, *i.e.* BSA, have shown to be crucial parameters. As a consequence, release in an acidic environment is completely retarded while in pH neutral surrounding occurred at very low rates (3 and 8% in the case of PBS or PBS + lipase respectively). When *P. aeruginosa* CFE in PBS was used as a degradation medium, significant increase of degradation and release were observed after one day only (13%). Although different coating materials have been developed so far, according to our knowledge they do not offer such slow and prolonged release of the antimicrobial agent in physiological conditions and fast release in adequate bacterial surroundings and during the foreign body reaction to implant. It was confirmed that SeNPs, as well as PCL/SeNPs, were effective in inhibiting *S. aureus* and *S. epidermidis*, the main causes

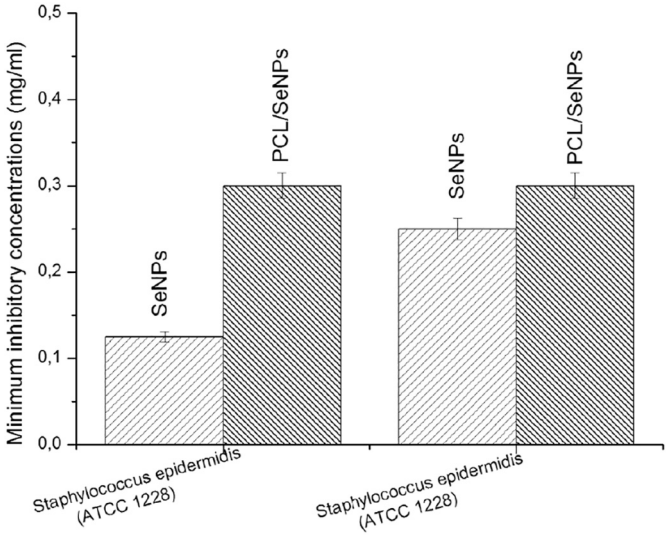

Fig. 10. Minimum inhibitory concentrations of SeNPs and PCL/SeNPs against two bacterial strains *S. aureus* and *S. epidermidis*.

of infections in orthopedics. Also, it was found that the particles possessed good biocompatibility since they showed no cytotoxicity, a low potential for ROS generation and a low genotoxicity potential. All these results imply that these designed particles could be a highly attractive and efficient platform for preventing infection on implants.

Acknowledgments

This study was supported by the Ministry of Education, Science and Technological Development of the Republic of Serbia, under Grants No. III45004, III43009, OI173048, and OI175102. The authors would like to thank Dr. Vladimir Pavlović and Dr. Ines Bračko for the microscopy characterization of the samples, Dr. Aleksandar Marinković for the FTIR measurements and Dr. Marina Milenković for determination of antibacterial properties. This work is supported by a European Science Foundation COST Action CA15114, a bilateral collaboration between Serbia and Slovenia (BI-RS/16-17-039) and Slovenian Research Agency: Program P1-0245. This work is also supported by the Italian Ministry of Foreign Affairs and International Cooperation (MAECI) within the collaboration framework between Italy and the Republic of Serbia (project PGR02952, call “Grande Rilevanza”).

Appendix A. Supplementary data

Supplementary data to this article can be found online at https://doi.org/10.1016/j.msec.2018.11.073.

References

[1] M. Navarro, A. Michiardi, O. Castan, J.A. Planell, Review. Biomaterials in orthopaedics, J. R. Soc. Interface (2008), https://doi.org/10.1098/rsif.2008.0151.
[2] J.M. Anderson, A. Rodriguez, D.T. Chang, Foreign body reaction to biomaterials, Semin. Immunol. 20 (2008) 86–100, https://doi.org/10.1016/j.smim.2007.11.004.
[3] R. Mittal, J. Morley, H. Dinopoulos, E.G. Drakoulakis, E. Vermani, P.V. Giannoudis, Use of bio-resorbable implants for stabilisation of distal radius fractures: the United Kingdom patients' perspective, Injury 36 (2005) 333–338, https://doi.org/10.1016/j.injury.2004.09.015.
[4] M. Zilberman, J.J. Elsner, Antibiotic-eluting medical devices for various applications, J. Control. Release 130 (2008) 202–215, https://doi.org/10.1016/j.jconrel.2008.05.020.
[5] N.N. Showan, M.Y., Jonathan Anne P., Sterility and infection, in: R. Narayan (Ed.), Biomed. Mater, Springer US, New York, 2009, pp. 239–258, , https://doi.org/10.1007/978-0-387-84872-3.
[6] E.C. Rodríguez-Merchán, A.D. Liddle, Microbiological concepts of the infected total knee arthroplasty, in: E.C. Rodríguez-Merchán, S. Oussedik (Eds.), Infected Total Knee Arthroplast, Springer, Cham, 2018, pp. 11–17, , https://doi.org/10.1007/978-3-319-66730-0_2.
[7] M. Ribeiro, F.J. Monteiro, M.P. Ferraz, Infection of orthopedic implants with emphasis on bacterial adhesion process and techniques used in studying bacterial-material interactions, Biomaterials 2 (2012) 176–194, https://doi.org/10.4161/biom.22905.
[8] D. Teterycz, T. Ferry, D. Lew, R. Stern, M. Assal, P. Hoffmeyer, L. Bernard, I. Uçkay, Outcome of orthopedic implant infections due to different staphylococci, Int. J. Infect. Dis. 14 (2010), https://doi.org/10.1016/j.ijid.2010.05.014.
[9] D.J. Evans, S.M.J. Fleiszig, Why does the healthy cornea resist *Pseudomonas aeruginosa* infection? Am J. Ophthalmol. 155 (2013) 961–970, https://doi.org/10.1016/j.ajo.2013.03.001.
[10] J. Yayan, B. Ghebremedhin, K. Rasche, Antibiotic resistance of *Pseudomonas aeruginosa* in pneumonia at a single University Hospital Center in Germany over a 10-year period, PLoS One 54 (2015) 1–20, https://doi.org/10.1371/journal.pone.0139836.
[11] J.A. Wright, S.P. Nair, Interaction of staphylococci with bone, Int. J. Med. Microbiol. 300 (2010) 193–204, https://doi.org/10.1016/j.ijmm.2009.10.003.
[12] S. Xie, Y. Tao, Y. Pan, W. Qu, G. Cheng, L. Huang, D. Chen, X. Wang, Z. Liu, Z. Yuan, Biodegradable nanoparticles for intracellular delivery of antimicrobial agents, J. Control. Release 187 (2014) 101–117, https://doi.org/10.1016/j.jconrel.2014.05.034.
[13] L. Zhao, P.K. Chu, Y. Zhang, Z. Wu, Antibacterial coatings on titanium implants, J Biomed Mater Res B Appl Biomater 91 (2009) 470–480, https://doi.org/10.1002/jbm.b.31463.
[14] C.M. Oliphant, K. Eroschenko, Antibiotic resistance, part 2: gram-negative pathogens, J. Nurs. Pract. 11 (2015) 79–86, https://doi.org/10.1016/j.nurpra.2014.10.008.
[15] C.M. Oliphant, K. Eroschenko, Antibiotic resistance, part 1: gram-positive pathogens, J. Nurs. Pract. 11 (2015) 70–78, https://doi.org/10.1016/j.nurpra.2014.09.018.
[16] P.A. Tran, T.J. Webster, Antimicrobial selenium nanoparticle coatings on polymeric medical devices, Nanotechnology 24 (2013), https://doi.org/10.1088/0957-4484/24/15/155101 (7 pp).
[17] M. Stevanović, V. Uskoković, M. Filipović, S.D. Škapin, D. Uskoković, Composite PLGA/AgNpPGA/AscH nanospheres with combined osteoinductive, antioxidative, and antimicrobial activities, ACS Appl. Mater. Interfaces 5 (2013) 9034–9042, https://doi.org/10.1021/am402237g.
[18] S. Shoeibi, M. Mashreghi, Biosynthesis of selenium nanoparticles using *Enterococcus faecalis* and evaluation of their antibacterial activities, J. Trace Elem. Med. Biol. 39 (2017) 135–139, https://doi.org/10.1016/j.jtemb.2016.09.003.
[19] E. Cremonini, E. Zonaro, M. Donini, S. Lampis, M. Boaretti, S. Dusi, P. Melotti, M.M. Lleo, G. Vallini, Biogenic selenium nanoparticles: characterization, antimicrobial activity and effects on human dendritic cells and fibroblasts, Microb. Biotechnol. 9 (2016) 758–771, https://doi.org/10.1111/1751-7915.12374.
[20] P.A. Tran, N. O'Brien-Simpson, E.C. Reynolds, N. Pantarat, D.P. Biswas, A.J. O'Connor, Low cytotoxic trace element selenium nanoparticles and their differential antimicrobial properties against *S. aureus* and *E. coli*, Nanotechnology 27 (2015) 045101, , https://doi.org/10.1088/0957-4484/27/4/045101.
[21] G. Guisbiers, Q. Wang, E. Khachatryan, L.C.C. Mimun, R. Mendoza-Cruz, P. Larese-Casanova, T.J.J. Webster, K.L.L. Nash, Inhibition of *E. coli* and *S. aureus* with selenium nanoparticles synthesized by pulsed laser ablation in deionized water, Int. J. Nanomedicine 11 (2016) 3731–3736, https://doi.org/10.2147/IJN.S106289.
[22] M. Roman, P. Jitaru, C. Barbante, Selenium biochemistry and its role for human health, Metallomics 6 (2014) 25–54, https://doi.org/10.1039/C3MT00185G.
[23] P.R. Hoffmann, M.J. Berry, The influence of selenium on immune responses, Mol. Nutr. Food Res. 52 (2008) 1273–1280, https://doi.org/10.1002/mnfr.200700330.
[24] M. Stevanović, N. Filipović, J. Djurdjević, M. Lukić, M. Milenković, A. Boccaccini, 45S5Bioglass®-based scaffolds coated with selenium nanoparticles or with poly (lactide-co-glycolide)/selenium particles: processing, evaluation and antibacterial activity, Colloids Surf. B: Biointerfaces 132 (2015) 208–215, https://doi.org/10.1016/j.colsurfb.2015.05.024.
[25] H. Zeng, J.J. Cao, G.F. Combs, Selenium in bone health: roles in antioxidant protection and cell proliferation, Nutrients 5 (2013) 97–110, https://doi.org/10.3390/nu5010097.
[26] R. Moreno-Reyes, D. Egrise, J. Nève, J.L. Pasteels, A. Schoutens, Selenium deficiency-induced growth retardation is associated with an impaired bone metabolism and osteopenia, J. Bone Miner. Res. 16 (2001) 1556–1563, https://doi.org/10.1359/jbmr.2001.16.8.1556.
[27] J.J. Cao, B.R. Gregoire, H. Zeng, Selenium deficiency decreases antioxidative capacity and is detrimental to bone microarchitecture in mice, J. Nutr. 142 (2012) 1526–1531, https://doi.org/10.3945/jn.111.157040.
[28] M. Vinceti, J. Mandrioli, P. Borella, B. Michalke, A. Tsatsakis, Y. Finkelstein, Selenium neurotoxicity in humans: bridging laboratory and epidemiologic studies, Toxicol. Lett. 230 (2014) 295–303, https://doi.org/10.1016/j.toxlet.2013.11.016.
[29] J.S. Morris, S.B. Crane, Selenium toxicity from a misformulated dietary supplement, adverse health effects, and the temporal response in the nail biologic monitor, Nutrients 5 (2013) 1024–1057, https://doi.org/10.3390/nu5041024.
[30] H. Wang, J. Zhang, H. Yu, Elemental selenium at nano size possesses lower toxicity without compromising the fundamental effect on selenoenzymes: comparison with selenomethionine in mice, Free Radic. Biol. Med. 42 (2007) 1524–1533, https://doi.org/10.1016/j.freeradbiomed.2007.02.013.
[31] J.S. Zhang, X.Y. Gao, L.D. Zhang, Y.P. Bao, Biological effects of a nano red elemental selenium, Biofactors 15 (2001) 27–38, https://doi.org/10.1002/biof.5520150103.
[32] M.A. Woodruff, D.W. Hutmacher, The return of a forgotten polymer - polycaprolactone in the 21st century, Prog. Polym. Sci. 35 (2010) 1217–1256, https://doi.org/10.1016/j.progpolymsci.2010.04.002.

[33] T.K. Dash, V.B. Konkimalla, Poly-ε-caprolactone based formulations for drug delivery and tissue engineering: a review, J. Control. Release 158 (2012) 15–33, https://doi.org/10.1016/j.jconrel.2011.09.064.
[34] V.R. Sinha, K. Bansal, R. Kaushik, R. Kumria, A. Trehan, Poly-ε-caprolactone microspheres and nanospheres: an overview, Int. J. Pharm. 278 (2004) 1–23, https://doi.org/10.1016/j.ijpharm.2004.01.044.
[35] L. Roseti, V. Parisi, M. Petretta, C. Cavallo, G. Desando, I. Bartolotti, B. Grigolo, Scaffolds for bone tissue engineering: state of the art and new perspectives, Mater. Sci. Eng. C 78 (2017) 1246–1262, https://doi.org/10.1016/j.msec.2017.05.017.
[36] M. Dhanka, C. Shetty, R. Srivastava, Injectable methotrexate loaded polycaprolactone microspheres: physicochemical characterization, biocompatibility, and hemocompatibility evaluation, Mater. Sci. Eng. C 81 (2017) 542–550, https://doi.org/10.1016/j.msec.2017.08.055.
[37] M. Kaur, S. Sharma, V.R. Sinha, Polymer based microspheres of aceclofenac as sustained release parenterals for prolonged anti-inflammatory effect, Mater. Sci. Eng. C 72 (2017) 492–500, https://doi.org/10.1016/j.msec.2016.11.092.
[38] V. Crescenzi, G. Manzini, G. Calzolari, C. Borri, Thermodynamics of fusion of poly-β-propiolactone and poly-ε-caprolactone. Comparative analysis of the melting of aliphatic polylactone and polyester chains, Eur. Polym. J. 8 (1972) 449–463, https://doi.org/10.1016/0014-3057(72)90109-7.
[39] T. Mosmann, Rapid colorimetric assay for cellular growth and survival: application to proliferation and cytotoxicity assays, J. Immunol. Methods 65 (1983) 55–63, https://doi.org/10.1016/0022-1759(83)90303-4.
[40] Š. Alja, M. Filipič, M. Novak, B. Žegura, Double strand breaks and cell-cycle arrest induced by the cyanobacterial toxin cylindrospermopsin in HepG2 cells, Mar. Drugs. 11 (2013) 3077–3090, https://doi.org/10.3390/md11083077.
[41] A. Štraser, M. Filipič, I. Gorenc, B. Žegura, The influence of cylindrospermopsin on oxidative DNA damage and apoptosis induction in HepG2 cells, Chemosphere 92 (2013) 24–30, https://doi.org/10.1016/j.chemosphere.2013.03.023.
[42] A. Štraser, M. Filipič, B. Žegura, Genotoxic effects of the cyanobacterial hepatotoxin cylindrospermopsin in the HepG2 cell line, Arch. Toxicol. 85 (2011) 1617–1626, https://doi.org/10.1007/s00204-011-0716-z.
[43] H.G. Schlegel, H. Kaltwasser, G. Gottschalk, Ein Submersverfahren zur Kultur wasserstoffoxydierender Bakterien: Wachstumsphysiologische Untersuchungen, Arch. Mikrobiol. 38 (1961) 209–222, https://doi.org/10.1007/BF00422356.
[44] M.M. Bradford, A rapid and sensitive method for quantitation of microgram quantities of protein utilizing the principle of protein-dye-binding, Anal. Biochem. 72 (1976) 248–254, https://doi.org/10.1016/0003-2697(76)90527-3.
[45] T. Teeraphatpornchai, T. Nakajima-Kambe, Y. Shigeno-Akutsu, M. Nakayama, N. Nomura, T. Nakahara, H. Uchiyama, Isolation and characterization of a bacterium that degrades various polyester-based biodegradable plastics, Biotechnol. Lett. 25 (2003) 23–28, https://doi.org/10.1023/A:1021713711160.
[46] S. Vasilijić, D. Savić, S. Vasilev, D. Vučević, S. Gašić, I. Majstorović, S. Janković, M. Čolić, Dendritic cells acquire tolerogenic properties at the site of sterile granulomatous inflammation, Cell. Immunol. 233 (2005) 148–157, https://doi.org/10.1016/j.cellimm.2005.04.007.
[47] P. Wayne, Clinical and Laboratory Standards Institute/NCCLS. Performance standards for antimicrobial susceptibility testing; fifteenth informational supplement. CLSI/NCCLS document M100-S15, Clin Lab Stand Inst. 25 (2005) 1–167.
[48] P. Kolhar, S. Mitragotri, Polymer microparticles exhibit size and shape dependent accumulation around the nucleus after endocytosis, Adv. Funct. Mater. 22 (2012) 3759–3764, https://doi.org/10.1002/adfm.201102918.
[49] Y. He, K. Park, Effects of the microparticle shape on cellular uptake, Mol. Pharm. 13 (2016) 2164–2171, https://doi.org/10.1021/acs.molpharmaceut.5b00992.
[50] H. Hillaireau, P. Couvreur, Nanocarriers' entry into the cell: relevance to drug delivery, Cell. Mol. Life Sci. 66 (2009) 2873–2896, https://doi.org/10.1007/s00018-009-0053-z.
[51] J.R. Weiser, W.M. Saltzman, Controlled release for local delivery of drugs: barriers and models, J. Control. Release 190 (2014) 664–673, https://doi.org/10.1016/j.jconrel.2014.04.048.
[52] FDA, 21 CFR 101 Food Labeling: Revision of the Nutrition and Supplement Facts Labels, 5100 Paint Branch Pkwy., College Park, https://www.federalregister.gov/documents/2016/05/27/2016-11867/food-labeling-revision-of-the-nutrition-and-supplement-facts-labels, (2016) , Accessed date: 19 November 2018.
[53] Institute of Medicine Food and Nutrition Board, Dietary Reference Intakes for Vitamin C, Vitamin E, Selenium, and Carotenoids, National Academies Press, Washington, D.C., 2000, https://doi.org/10.17226/9810.
[54] N. Filipović, M. Stevanović, A. Radulović, V. Pavlović, D. Uskoković, Facile synthesis of poly(ε-caprolactone) micro and nanospheres using different types of polyelectrolytes as stabilizers under ambient and elevated temperature, Compos. Part B 45 (2013) 1471–1479, https://doi.org/10.1016/J.COMPOSITESB.2012.07.008.
[55] E. Verderio, A. Coombes, R.A. Jones, X. Li, D. Heath, S. Downes, M. Griffin, A new type of surgical adhesive made from porcine collagen and polyglutamic acid, J. Biomed. Mater. Res. 54 (2001) 305–310, https://doi.org/10.1002/1097-4636(200102)54:2<305::AID-JBM18>3.0.CO;2-B.
[56] A. Ogunleye, A. Bhat, V.U. Irorere, D. Hill, C. Williams, I. Radecka, Poly-γ-glutamic acid: production, properties and applications, Microbiology 161 (2015) 1–17, https://doi.org/10.1099/mic.0.081448-0.
[57] N. Filipović, M. Stevanović, J. Nunić, S. Cundrič, M. Filipič, D. Uskoković, Synthesis of poly(ε-caprolactone) nanospheres in the presence of the protective agent poly (glutamic acid) and their cytotoxicity, genotoxicity and ability to induce oxidative stress in HepG2 cells, Colloids Surf. B: Biointerfaces 117 (2014) 414–424, https://doi.org/10.1016/J.COLSURFB.2014.03.015.
[58] J. Grdadolnik, Y. Maréchal, Bovine serum albumin observed by infrared spectrometry. II. Hydration mechanisms and interaction configurations of embedded H_2O molecules, Biopolym. - Biospectroscopy Sect. 62 (2001) 54–67, https://doi.org/10.1002/(SICI)1097-0282(200007)54:1<64::AID-BIP70>3.0.CO;2-R.
[59] I. Castilla-Cortázar, J. Más-Estellés, J.M. Meseguer-Dueñas, J.L. Escobar Ivirico, B. Marí, A. Vidaurre, Hydrolytic and enzymatic degradation of a poly(ε-caprolactone) network, Polym. Degrad. Stab. 97 (2012) 1241–1248, https://doi.org/10.1016/j.polymdegradstab.2012.05.038.
[60] G. Sekosan, N. Vasanthan, Morphological changes of annealed poly-ε-caprolactone by enzymatic degradation with lipase, J. Polym. Sci. B Polym. Phys. 48 (2010) 202–211, https://doi.org/10.1002/polb.21889.
[61] J.C. Jeong, J. Lee, K. Cho, Effects of crystalline microstructure on drug release behavior of poly(ε-caprolactone) microspheres, J. Control. Release 92 (2003) 249–258, https://doi.org/10.1016/S0168-3659(03)00367-5.
[62] S. Dwivedi, A.A. Alkhedhairy, M. Ahamed, J. Musarrat, Biomimetic synthesis of selenium nanospheres by bacterial strain JS-11 and its role as a biosensor for nanotoxicity assessment: a novel se-bioassay, PLoS One 8 (2013) 1–10, https://doi.org/10.1371/journal.pone.0057404.
[63] A.H. Pinto, E.R. Leite, E. Longo, E.R. De Camargo, Crystallization at room temperature from amorphous to trigonal selenium as a byproduct of the synthesis of water dispersible zinc selenide, Mater. Lett. 87 (2012) 62–65, https://doi.org/10.1016/j.matlet.2012.07.067.
[64] X. Wang, Y. Wang, K. Wei, N. Zhao, S. Zhang, J. Chen, Drug distribution within poly (ε-caprolactone) microspheres and in vitro release, J. Mater. Process. Technol. 209 (2009) 348–354, https://doi.org/10.1016/j.jmatprotec.2008.02.004.
[65] T. Estey, J. Kang, S.P. Schwendeman, J.F. Carpenter, BSA degradation under acidic conditions: a model for protein instability during release from PLGA delivery systems, J. Pharm. Sci. 95 (2006) 1626–1639, https://doi.org/10.1002/jps.20625.
[66] C. Wu, T.F. Jim, Z. Gan, Y. Zhao, S. Wang, A heterogeneous catalytic kinetics for enzymatic biodegradation of poly(ε-caprolactone) nanoparticles in aqueous solution, Polymer (Guildf). 41 (2000) 3593–3597, https://doi.org/10.1016/S0032-3861(99)00586-8.
[67] J.S. Chawla, M.M. Amiji, Biodegradable poly(ε-caprolactone) nanoparticles for tumor-targeted delivery of tamoxifen, Int. J. Pharm. 249 (2002) 127–138, https://doi.org/10.1016/S0378-5173(02)00483-0.
[68] S. Niiyama, R. Happle, R. Hoffmann, Validation of patient-reported outcomes measurement information system (PROMIS) short forms for use in childhood-onset systemic lupus erythematosus, Eur. J. Dermatol. 11 (2001) 475–476, https://doi.org/10.1002/acr.
[69] A. Muñoz-Bonilla, M. Fernández-García, Polymeric materials with antimicrobial activity, Prog. Polym. Sci. 37 (2012) 281–339, https://doi.org/10.1016/j.progpolymsci.2011.08.005.